

This work has been submitted to the *IEEE Transactions on Signal Processing* for possible publication. Copyright may be transferred without notice, after which this version may no longer be accessible.

Foundations of MIMO Radar Detection Aided by Reconfigurable Intelligent Surfaces

Stefano Buzzi, *Senior Member, IEEE*, Emanuele Grossi, *Senior Member, IEEE*, Marco Lops, *Fellow, IEEE*, Luca Venturino, *Senior Member, IEEE*

Abstract—A reconfigurable intelligent surface (RIS) is a flat layer made of sub-wavelength-sized reflective elements capable of adding a tunable phase shift to the impinging electromagnetic wave. This paper considers the fundamental problem of target detection in a RIS-aided multiple-input multiple-output (MIMO) radar system. At first, a general signal model is introduced, which includes the possibility of using up to two RISs (one close to the transmitter and one close to the receiver) and subsumes both a mono-static and a bi-static radar configuration with or without a line-of-sight (LOS) view of the prospective target. Upon resorting to a generalized likelihood ratio test (GLRT), the design of the RIS phase shifts is formulated as the maximization of the probability of detection in the resolution cell under inspection for a fixed probability of false alarm, and suitable optimization algorithms are proposed and discussed. Both the theoretical and the numerical analysis clearly show the benefits, in terms of the signal-to-noise ratio (SNR) at the radar receiver, granted by the use of the RISs and shed light on the interplay among the key system parameters, such as the radar-RIS distance, the RIS size, and location of the prospective target. A major finding is that the RISs should be deployed in the near-field of the radar transmit/receive array. The paper is then concluded by discussing some open problems and foreseen applications.

Index Terms—MIMO Radar, LOS/NLOS, Bi/Mono-Static, Target Detection, Reconfigurable Intelligent Surfaces, Metasurfaces.

I. INTRODUCTION

A reconfigurable intelligent surface (RIS) is an emerging technology that has recently attracted a huge interest from both academic and industry researchers in the wireless communications and sensing community [1]–[3]. An RIS is a planar structure that is made of engineered material with tunable electromagnetic characteristics that can be controlled to alter the wireless propagation environment [4]–[6]. Over the last few years, the RISs have been widely investigated in wireless communications, with the aim of understanding how and to what extent they could enhance the networks performance. In [7], the RIS is modeled as an array of reflecting elements with tunable phase shifts and, with reference to a base station (BS) serving several downlink devices, the transmit power and

the phase shifts are jointly designed to maximize the energy efficiency. In [8], an indoor environment is considered and a deep neural network able to learn the mapping between the position of the users and the RIS phase shifts is designed, so as to maximize the signal strength at the user’s location. The work in [9] assumes that the phase shifts of the RIS elements can take value in a finite set and investigates the relation between the set cardinality and the rate degradation. In [10], the RIS phase shifts are exploited in conjunction with the communication transmitter to encode a message, and it is shown that this scheme achieves a larger capacity than that obtained when the RIS is designed only to maximize the signal-to-noise ratio (SNR) at the receiver. The work in [11], instead, considers a point-to-point multiple-input multiple-output (MIMO) link and, accounting for the finite alphabet input, performs an alternating optimization of the transmit precoder and RIS phase shifts to minimize the symbol error rate. The problem of channel estimation in RIS-aided wireless communications has been tackled in [12]–[14], while other studies have assessed the RIS benefits in the context of wireless power transfer [15], non-orthogonal multiple access [16], design of innovative antenna configurations [17], and coverage extension [18]. The reader may refer to [1]–[3] and the references therein for a more comprehensive overview.

The RIS potentials have been also investigated in positioning and localization tasks, as discussed in [19]. In [20], a scenario with one BS, one mobile device, and one RIS is considered, and the problem of finding the device position and orientation is discussed; the Cramer-Rao lower bounds to the estimation error are computed and the RIS configuration maximizing the sum of the SNRs at each BS antenna is given. As shown in [21], the use of an RIS allows to perform joint synchronization and user localization without using two-way transmission, even if the mobile user is equipped with one antenna. In [22], a similar approach is pursued for the case that the BS has only one antenna, and joint three-dimensional localization and synchronization in a single-user multi-carrier system is addressed, under the assumption of line-of-sight (LOS) propagation and in the presence of a uniform planar reflecting array. Joint localization and communication is then addressed in [23], wherein a procedure to determine the RIS phase shifts based on the use of hierarchical codebooks and feedback from the mobile station is presented.

In the last few months, the possible benefits that the RISs can bring to radar systems and to the spectral coexistence between radar and communication have started being investigated. The work in [24] exploits an RIS to enhance

The authors are planning to submit part of this work at the 25th International ITG Workshop on Smart Antennas (WSA 2021).

S. Buzzi, E. Grossi and L. Venturino are with the Department of Electrical and Information Engineering (DIEI), University of Cassino and Southern Lazio, 03043 Cassino, Italy, and with Consorzio Nazionale Interuniversitario per le Telecomunicazioni, 43124 Parma, Italy (e-mail: buzzi@unicas.it; e.grossi@unicas.it; l.venturino@unicas.it).

M. Lops is with the Department of Electrical and Information Technology (DIETI), University of Naples Federico II, 80138 Naples, Italy, and with Consorzio Nazionale Interuniversitario per le Telecomunicazioni, 43124 Parma, Italy (e-mail: lops@unina.it).

the sensing and communication capabilities of a mmWave dual function transceiver; here, separate RIS elements are used for sensing and communication, and a two-dimensional hierarchical codebook for the RIS configuration is presented, along with a method to choose the number of snapshots used in each stage to get a desired target localization performance. In [25], a dual function system is again considered, and the radar detection probability is maximized by optimizing the BS transmit beamformer and the RIS phase shifts, subject to signal-to-interference-plus-noise-ratio and power consumption constraints. A similar approach is pursued in [26], wherein the design of the phase shifts and of the precoding matrix of an RIS-aided BS is considered, which is carried out by maximizing the SNR at the radar receiver subject to sensing and communication constraints. Finally, the transmitted waveform and the RIS configuration are chosen in [27] to mitigate the multiuser interference under a beam pattern constraint.

With regard to the target detection problem, in our earlier contribution [28] we assumed that the radar is capable of forming (a) two transmit beams pointing towards the prospective target and the RIS and one receive beam pointing towards the prospective target only or, viceversa, (b) one transmit beam pointing towards the prospective target only and two receive beams pointing towards the prospective target and the RIS. Under such a scenario, a theoretical analysis is carried out for closely- and widely-spaced (with respect to the location of the prospective target) radar and RIS deployments, showing that large gains can be provided by the nearby RIS, and initial hints on the optimal RIS placement are provided. In [29], the case where no direct path between the radar and the prospective target exists is considered, mimicking the companion situation where the RIS provides an indirect link between a communication source and a destination that would be otherwise not reachable. Finally, [30] represents a first contribution to the scenario considered here and, although passing over a number of relevant effects and situations, as detailed in the sequel of this contribution, makes the basic point that an RIS can indeed aid the radar detection.

A. Contribution and paper structure

The bottom line of the current studies is that suitably deployed RISs modify the wireless channel response, thus providing novel degrees of freedom to design wireless systems. In this context, we aim at investigating if and under which conditions the RISs may boost the performance of a radar, by focusing on the classical target detection problem. With reference to the scenarios outlined in Fig. 1, we first derive a truly general and novel signal model, wherein a MIMO radar transmits a set of orthogonal waveforms and, assisted by a *forward* and/or a *backward* RIS, verifies the presence/absence of a prospective target in a given resolution cell under inspection. The considered model includes mono-static, bi-static, LOS, and non-line-of-sight (NLOS) radar configurations and accounts for the presence of up to four paths from the transmitter to the prospective target to the receiver. Also, we distinguish among the two relevant situations that the forward and backward RISs are in the near or far-field of the transmitter and receiver, respectively.

Next, we derive the generalized likelihood ratio test (GLRT) receiver with respect to the unknown target response and tackle the design of the phase shifts of the reflecting elements by maximizing the target detection probability for a fixed probability of false alarm: interestingly, the optimization problem turns out to be *separable*, i.e., the forward and backward RISs can be designed independently. Also, if the forward (backward) RIS and radar transmitter (receiver) are in each other's far-field the optimum phase shifts are found in closed form; instead, in a near-field situation, the optimization problem is strongly NP-hard in general and is approximately solved through either an alternate maximization or by resorting to a convex relaxation. Interestingly, this latter approach provides a randomized solution whose expected value is at least $\pi/4 \approx 0.785$ times the optimum. The special case in which the radar is mono-static and there is only one RIS providing a forward and a backward indirect path is also examined, and an ad-hoc algorithm to select the phase shift of each reflecting element is proposed.

The theoretical analysis shows that only a marginal gain (as compared to the case where the radar operates alone) can be obtained if radar and RIS are in each other's far-field. This confirms the intuition in [28] that an RIS should be better placed in proximity of the radar transmitter or receiver, unless a far-field deployment is necessary to inspect a NLOS spot that would otherwise remain blind [29]. An extensive numerical analysis is also provided, aimed at assessing the impact of the radar-RIS distance, the RIS size, and the location of the inspected cell. The results show that a large gain can be obtained under a near-field radar-RIS deployment; interestingly, such gain almost doubles when the prospective target is in the view of both the forward and the backward RIS, as compared to the case where only a single surface can illuminate/observe it. The performance of a mono-static radar with a single RIS (the simplest and perhaps most realistic and cost-effective configuration) is also contrasted to that of an *ideal* system where the phase shifts of the reflecting elements are changed in between the transmission and reception phases, showing that these configurations are substantially equivalent.

The paper is organized as follows. In Sec. II, the system description and the modelling assumptions are presented. In Sec. III, the design of the phase shifts introduced by the reflecting elements of the RISs is studied. In Sec. IV, some numerical examples are given to illustrate the advantages of using an RIS-aided radar. Finally, concluding remarks and hints for future developments are provided in Sec. V.

B. Notation

Column vectors and matrices are denoted by lowercase and uppercase boldface letters, respectively. The symbols $(\cdot)^*$, $(\cdot)^T$ and $(\cdot)^H$ denote the conjugate, the transpose, and the conjugate-transpose operation, respectively. \mathbf{I}_M is a $M \times M$ identity matrix, while A_{ij} and a_i denote the (i, j) -th entry of the matrix \mathbf{A} and the i -th entry of the vector \mathbf{a} , respectively. $\mathbf{A} \succeq 0$ means that \mathbf{A} is Hermitian positive semidefinite. $\text{tr}\{\mathbf{A}\}$ and $\|\mathbf{a}\|$ denote the trace of the square matrix \mathbf{A} and the Frobenius norm of the vector \mathbf{a} , respectively, while $\text{Rank}\{\mathbf{A}\}$

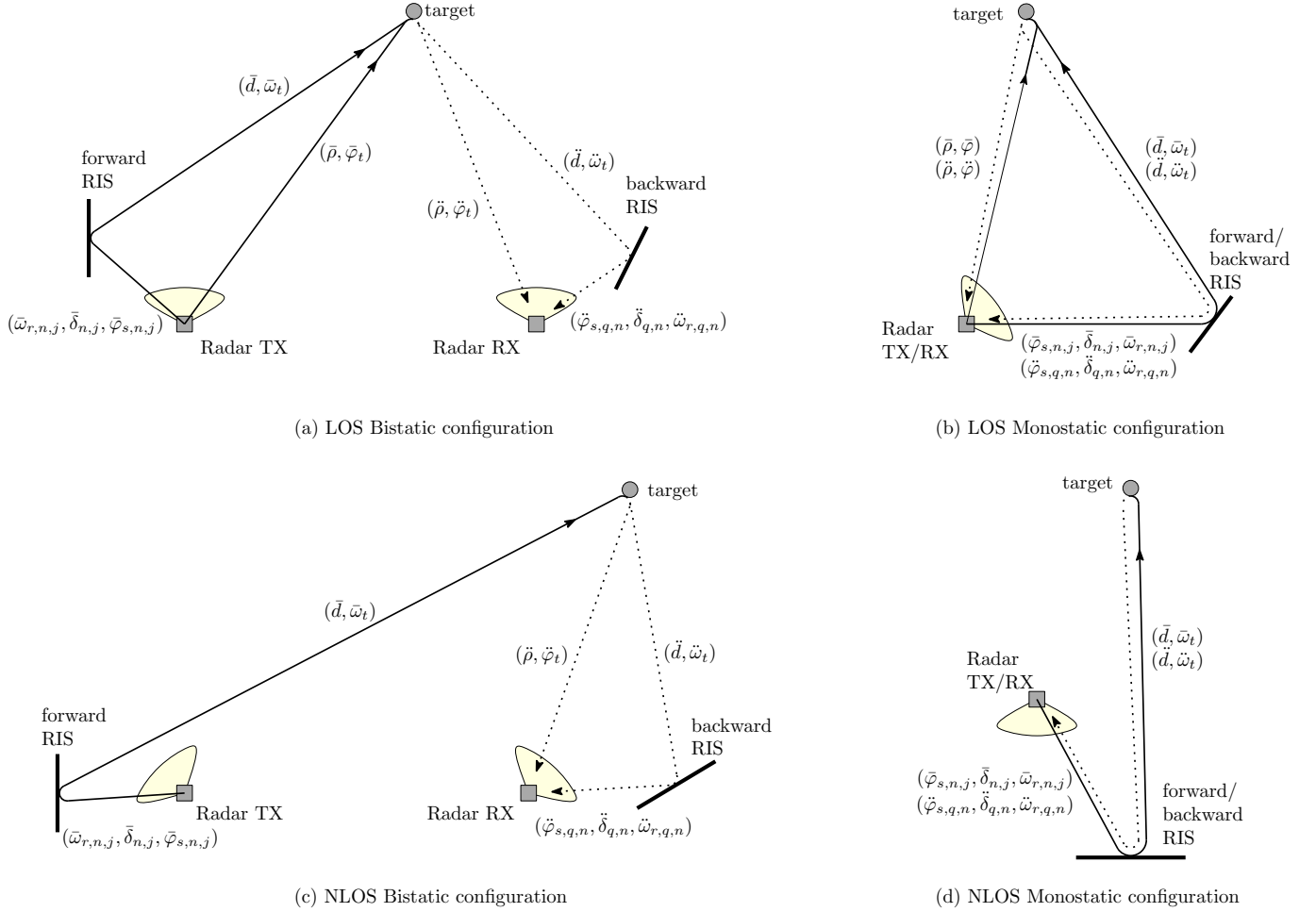


Figure 1. Examples of system geometries.

is the rank of the matrix \mathbf{A} . $\text{vec}\{\mathbf{a}_1, \dots, \mathbf{a}_N\}$ is the MN -dimensional vector obtained by piling up the M -dimensional vectors $\{\mathbf{a}_n\}_{n=1}^N$. $\text{diag}\{\mathbf{a}\}$ is the $M \times M$ matrix containing the entries of M -dimensional vector \mathbf{a} on the main diagonal and zero elsewhere. The symbol \otimes denotes the Kronecker product, $E[\cdot]$ the statistical expectation, and i the imaginary unit.

II. SYSTEM DESCRIPTION

We consider a radar system aimed at detecting a prospective target in a given resolution cell under inspection. The radar is equipped with a transmitter and a receiver with $\bar{N}_r \geq 1$ and $\bar{N}_r \geq 1$ closely-spaced elements, respectively, arranged into a planar array; the building element of each array can be a single antenna or a subarray module composed itself of multiple antennas. The radar operates with a carrier wavelength λ and emits \bar{N}_r orthogonal and equal-power waveforms, one from each radiating element.¹ A nearby RIS (referred to as the forward RIS) helps the transmitter illuminate the prospective target; this surface is composed of $\bar{N}_s \geq 1$ closely-spaced reflecting elements of area \bar{A}_s , arranged into a planar array; we denote by $\bar{\varphi}_n$ the phase shift introduced by the n -th element, by $\bar{\varphi} = (\bar{\varphi}_1 \dots \bar{\varphi}_{\bar{N}_s})^\top$ the vectors containing all phase shifts,

¹The possible optimization of the radiated waveforms is not considered here and left as a future development.

and by $\bar{I}_s \in \{1, 0\}$ the indicator variable specifying if this RIS is present or not. Similarly, a nearby RIS (referred to as the backward RIS) helps the receiver capture the power scattered by the prospective target; this surface is composed of $\bar{N}_s \geq 1$ closely-spaced reflecting elements of area \bar{A}_s , arranged into a planar array; we denote by $\bar{\varphi}_n$ the phase shift introduced by the n -th element, by $\bar{\varphi} = (\bar{\varphi}_1 \dots \bar{\varphi}_{\bar{N}_s})^\top$ the vectors containing all phase shifts, and by $\bar{I}_s \in \{1, 0\}$ the indicator variable specifying if this RIS is present or not.

The RISs modify the response of the environment to the waveforms emitted by the radar [31]; a prospective target can be illuminated by the transmitter (direct path) and/or by the forward RIS (indirect path); likewise, the corresponding reflections originated by the target may reach the receiver through a direct path and/or an indirect path bouncing on the backward RIS. As shown in Fig. 1, up to four echoes may be observed, corresponding to a direct illumination and a direct reflection (e_{rr}), a indirect illumination and a direct reflection (e_{sr}), a direct illumination and a indirect reflection (e_{rs}), and a indirect illumination and a indirect reflection (e_{ss}). The considered model encompasses both a bi-static and a mono-static radar; in this latter case, the forward and backward RIS may collapse into a single surface redirecting both incident waves from the transmitter towards the target and from the

target towards the receiver, as shown in Figs. 1(b)-(d). Also, the model encompasses both a LOS and a NLOS radar; in the former case, both the transmitter and the receiver have a direct view of the inspected resolution cell and the indirect paths granted by the RIS can be exploited to improve the detection performance that the radar would have alone; in the latter case, either the transmitter or the receiver or both do not have a direct view of the inspected resolution cell and the indirect paths granted by the RISs extend the field of view of the radar, as shown in Figs. 1(c)-(d). We underline that the configuration in Fig. 1(d) may be of interest also to replace a possibly expensive radar transceiver that would be required to cover the region of interest with a low-cost feeder that sends/receives signals via a re-configurable surface capable of electronically-tunable beamforming [28].

A. Geometric parameters

Let \bar{O}_r , \ddot{O}_r , \bar{O}_s , and \ddot{O}_s be a Cartesian right-handed local reference system (LRS) placed at the transmitter, the receiver, the forward RIS, and the backward RIS, respectively. We assume that each array is on the (y, z) -plane of the corresponding LRS, with the array center located at the origin and each element oriented towards the positive x -axis. At the transmitter, we define the following quantities:

- $\bar{\rho}$, $\bar{\theta}_t^{\text{az}}$, and $\bar{\theta}_t^{\text{el}}$ are the range and the azimuth and elevation angles of the target in \bar{O}_r , respectively;²
- $\bar{\delta}$, $\bar{\theta}_s^{\text{az}}$, and $\bar{\theta}_s^{\text{el}}$ are the range and the azimuth and elevation angles of the center of the forward RIS in \bar{O}_r , respectively;
- $\bar{\delta}_{nj}$, $\bar{\theta}_{s,nj}^{\text{az}}$, and $\bar{\theta}_{s,nj}^{\text{el}}$ are the distance and the azimuth and elevation angles of the n -th forward reflecting element in the LRS obtained upon translating \bar{O}_r at the j -th transmit element, respectively; clearly, we have $\bar{\delta}_{nj} = \bar{\delta}$, $\bar{\theta}_{s,nj}^{\text{az}} = \bar{\theta}_s^{\text{az}}$, and $\bar{\theta}_{s,nj}^{\text{el}} = \bar{\theta}_s^{\text{el}}$ if the j -th transmit element and the n -th forward reflecting element are at the center of the corresponding array.

At the forward RIS, we define the following quantities:

- \bar{d} , $\bar{\omega}_t^{\text{az}}$, and $\bar{\omega}_t^{\text{el}}$ are the range and the azimuth and elevation angles of the target in \bar{O}_s , respectively;
- $\bar{\delta}$, $\bar{\omega}_r^{\text{az}}$, and $\bar{\omega}_r^{\text{el}}$ are the range and the azimuth and elevation angles of the center of the transmit array in \bar{O}_s , respectively;
- $\bar{\delta}_{nj}$, $\bar{\omega}_{r,nj}^{\text{az}}$, and $\bar{\omega}_{r,nj}^{\text{el}}$ are the range and the azimuth and elevation angles of the j -th transmit element in the LRS obtained upon translating \bar{O}_s at the n -th forward reflecting element.

Specular geometric parameters can be defined at the transmitter and the backward RIS with respect to \ddot{O}_r and \ddot{O}_s , respectively, with an obvious modification of the symbol notation (i.e., the overline is replaced with two dots). For

²We follow the standard notation that the azimuth angle of a point $\mathbf{p} \in \mathbb{R}^3$ is the angle between the x -axis and the orthogonal projection of the vector pointing towards \mathbf{p} onto the (x, y) -plane, which takes values in $[-\pi, \pi)$ and is positive when going from the x -axis towards the y -axis; also, the elevation angle is the angle between the vector pointing towards \mathbf{p} and its orthogonal projection onto the (x, y) -plane, which takes values in $[-\pi/2, \pi/2)$ and is positive when going toward the positive z -axis from the (x, y) -plane.

brevery, we denote by $\varphi = \{\varphi^{\text{az}}, \varphi^{\text{el}}\}$ the pair of azimuth and elevation angles φ^{az} and φ^{el} . For the reader's sake, the main geometric parameters are summarized in Fig. 1.

B. Design assumptions

At the design stage, we make the following assumptions.

- There is no coupling among the elements of each array.
- There is LOS propagation in the radar-RIS, radar-target, and RIS-target hops (whenever present).
- The waveforms are narrowband, so that the delays of the target echoes reaching the receiver are not resolvable.
- When both the transmitter and the forward RIS illuminate the prospective target, they see the same aspect angle [32], i.e., $\lambda/\bar{D}_t \gg \max_{n,j} \bar{\xi}_{nj}$, where \bar{D}_t is the effective size of the target as seen from the transmitter and $\bar{\xi}_{nj}$ is the angle formed by the line segment linking the target with the j -th transmit element and the line segment linking the target with the n -th forward reflecting element; similarly, when both the receiver and the backward RIS observe the prospective target, they see the same aspect angle, i.e., $\lambda/\ddot{D}_t \gg \max_{q,n} \ddot{\xi}_{qn}$, where \ddot{D}_t is the effective size of the target as seen from the receiver and $\ddot{\xi}_{qn}$ is the angle formed by the line segment linking the target with the q -th receive element and the line segment linking the target with the n -th backward reflecting element.
- The target and the forward (backward) RIS are in each other's far-field, i.e., we have [33]

$$\bar{d} \geq \max\{2\bar{D}_t^2/\lambda, 2\bar{D}_r^2/\lambda, 5\bar{D}_t, 5\bar{D}_s, 1.6\lambda\} \quad (1a)$$

$$\ddot{d} \geq \max\{2\ddot{D}_t^2/\lambda, 2\ddot{D}_s^2/\lambda, 5\ddot{D}_t, 5\ddot{D}_s, 1.6\lambda\} \quad (1b)$$

where \bar{D}_s and \ddot{D}_s are the maximum size of the forward and backward RISs, respectively; also, the target and each radar array are in each other's far-field, i.e., we have [33]

$$\bar{\rho} \geq \max\{2\bar{D}_t^2/\lambda, 2\bar{D}_r^2/\lambda, 5\bar{D}_t, 5\bar{D}_r, 1.6\lambda\} \quad (2a)$$

$$\bar{\rho} \geq \max\{2\ddot{D}_t^2/\lambda, 2\ddot{D}_r^2/\lambda, 5\ddot{D}_t, 5\ddot{D}_r, 1.6\lambda\} \quad (2b)$$

where \bar{D}_r and \ddot{D}_r are the maximum size of the transmit and the receive array, respectively. Accordingly, the phase curvature of the wavefront can be neglected along the radar-target and RIS-target hops [33], [34].

- Any pair of transmit and forward reflecting elements are in each other's far-field; similarly, any pair of receive and backward reflecting elements are in each other's far-field. This requires that [33]

$$\min_{n,j} \bar{\delta}_{nj} \geq \max\{2\bar{\Delta}_r^2/\lambda, 2\bar{\Delta}_s^2/\lambda, 5\bar{\Delta}_r, 5\bar{\Delta}_s, 1.6\lambda\} \quad (3a)$$

$$\min_{q,n} \ddot{\delta}_{qn} \geq \max\{2\ddot{\Delta}_r^2/\lambda, 2\ddot{\Delta}_s^2/\lambda, 5\ddot{\Delta}_r, 5\ddot{\Delta}_s, 1.6\lambda\} \quad (3b)$$

where $\bar{\Delta}_r$, $\bar{\Delta}_s$, $\ddot{\Delta}_r$, and $\ddot{\Delta}_s$ are the maximum size of each element of the transmit, forward reflecting, receive, and backward reflecting arrays, respectively. We underline that the transmitter and the forward RIS and, similarly, the receiver and the backward RIS are not required to be in each other's far-field. Accordingly, the phase curvature

of the wavefront across the array elements will not be neglected in the radar-RIS hops [17], [35].

C. Received signal

As customary, a range gating operation is at first performed by projecting the signal impinging on each receive element along a delayed version of each transmit waveform (this is tantamount to sampling the output of a filter matched to the waveform), with the delay tied to the distance of the inspected resolution cell from the transmitter and the receiver. Accordingly, a $\tilde{N}_r \times \tilde{N}_r$ observation matrix, say \mathbf{R} , is obtained, whose rows contains the \tilde{N}_r samples (one for each transmit element) taken at each of the \tilde{N}_r receive elements; in the presence of a steady target, this matrix can be modeled as

$$\mathbf{R} = \alpha \left(\underbrace{\tilde{\gamma}_r \tilde{\mathbf{v}}_r \tilde{\mathbf{v}}_r^T \tilde{\gamma}_r}_{\mathbf{E}_{rr}} + \underbrace{\tilde{\gamma}_r \tilde{\mathbf{v}}_r \tilde{\mathbf{v}}_s^T \bar{\mathbf{X}}(\bar{\varphi}) \bar{\mathbf{G}} \tilde{\gamma}_s}_{\mathbf{E}_{sr}(\bar{\varphi})} + \underbrace{\tilde{\gamma}_s \ddot{\mathbf{G}} \ddot{\mathbf{X}}(\ddot{\varphi}) \ddot{\mathbf{v}}_s \tilde{\mathbf{v}}_r^T \tilde{\gamma}_r}_{\mathbf{E}_{rs}(\ddot{\varphi})} \right. \\ \left. + \underbrace{\tilde{\gamma}_r \ddot{\mathbf{G}} \ddot{\mathbf{X}}(\ddot{\varphi}) \ddot{\mathbf{v}}_s \tilde{\mathbf{v}}_s^T \bar{\mathbf{X}}(\bar{\varphi}) \bar{\mathbf{G}} \tilde{\gamma}_s}_{\mathbf{E}_{ss}(\bar{\varphi}, \ddot{\varphi})} \right) + \mathbf{W} \quad (4)$$

where we have defined the following quantities.

- $\alpha \in \mathbb{C}$ is the unknown target response.
- $\tilde{\gamma}_r \in \mathbb{C}$ is the known channel between the reference transmit element (assumed to be located at the center of the array) and the target, which accounts for the radiated power, say \bar{P}_r , the transmit gain, the path-loss, and phase delay; $\tilde{\gamma}_s \in \mathbb{C}$ is the known channel from the reference transmit element to the reference forward reflecting element to the target, which also accounts for the bi-static radar cross-section (RCS) of the reflecting element.
- $\check{\gamma}_r \in \mathbb{C}$ is the known channel between the target and the reference receive element, which accounts for the receive gain, the path-loss, and phase delay; $\check{\gamma}_s \in \mathbb{C}$ is the known channel from the target to the reference backward reflecting element to the reference receive element, which also accounts for the bi-static RCS of the reflecting element.
- $\tilde{\mathbf{v}}_r \in \mathbb{C}^{\tilde{N}_r}$ ($\check{\mathbf{v}}_r \in \mathbb{C}^{\tilde{N}_r}$) is the *direct* transmit (receive) steering vector of the radar towards the direction $\bar{\theta}_t$ ($\check{\theta}_t$) of the target; $\tilde{\mathbf{v}}_s \in \mathbb{C}^{\tilde{N}_s}$ ($\check{\mathbf{v}}_s \in \mathbb{C}^{\tilde{N}_s}$) is the transmit (receive) steering vector of the forward (backward) RIS towards the direction $\bar{\omega}_t$ ($\check{\omega}_t$) of the target; these vectors are tied to the array geometry and have unit-magnitude entries.
- $\bar{\mathbf{X}}(\bar{\varphi}) = \text{diag}\{(e^{i\bar{\varphi}_1} \dots e^{i\bar{\varphi}_{N_s}})^T\} \in \mathbb{C}^{\tilde{N}_s \times \tilde{N}_s}$ and $\ddot{\mathbf{X}}(\ddot{\varphi}) = \text{diag}\{(e^{i\ddot{\varphi}_1} \dots e^{i\ddot{\varphi}_{\tilde{N}_s}})^T\} \in \mathbb{C}^{\tilde{N}_s \times \tilde{N}_s}$ are the matrices accounting for the phase response of the forward and backward reflecting elements, respectively.
- $\bar{\mathbf{G}} \in \mathbb{C}^{\tilde{N}_s \times \tilde{N}_r}$ and $\ddot{\mathbf{G}} \in \mathbb{C}^{\tilde{N}_r \times \tilde{N}_s}$ are the known channel matrices between the transmitter and the forward RIS and between the backward RIS and the receiver, respectively;
- Finally, $\mathbf{W} \in \mathbb{C}^{\tilde{N}_r \times \tilde{N}_r}$ is a matrix accounting for the additive disturbance, whose entries are modeled as independent and identically distributed (i.i.d.) circularly-symmetric Gaussian random variables with variance σ_w^2 .

Depending on the values of $\tilde{\gamma}_r$, $\tilde{\gamma}_s$, $\check{\gamma}_r$, and $\check{\gamma}_s$ only some of the echoes e_{rr} , e_{sr} , e_{rs} , and e_{ss} may be actually present:

Table I
POSSIBLE SYSTEM CONFIGURATIONS

Radar	$\tilde{\gamma}_r$	$\check{\gamma}_r$	$\tilde{\gamma}_s$	$\check{\gamma}_s$	Target	
					illuminated by	observed by
LOS	$\neq 0$	$\neq 0$	$\neq 0$	$\neq 0$	Radar & RIS	Radar & RIS
			$= 0$	$\neq 0$	Radar	Radar & RIS
			$\neq 0$	$= 0$	Radar & RIS	Radar
			$= 0$	$= 0$	Radar	Radar
NLOS	$\neq 0$	$= 0$	$\neq 0$	$\neq 0$	Radar & RIS	RIS
			$= 0$	$\neq 0$	Radar	RIS
			$= 0$	$= 0$	RIS	RIS
			$= 0$	$\neq 0$	RIS	Radar & RIS
			$\neq 0$	$= 0$	RIS	Radar

all possible system configurations are outlined in Table I. Finally, we point out that $\bar{\mathbf{G}}^T \bar{\mathbf{X}}(\bar{\varphi}) \tilde{\mathbf{v}}_s$ and $\ddot{\mathbf{G}} \ddot{\mathbf{X}}(\ddot{\varphi}) \check{\mathbf{v}}_s$ can be interpreted as the *indirect* transmit (receive) steering vector of the radar towards the target via the RIS-assisted path,³ which are controlled through the phases of the reflecting elements.

It is now convenient to reorganize the above model into a vector form; upon defining $\mathbf{r} = \text{vec}\{\mathbf{R}\} \in \mathbb{C}^{\tilde{N}_r \tilde{N}_r}$ and

$$e_{rr} = \text{vec}\{\mathbf{E}_{rr}\} = (\tilde{\gamma}_r \tilde{\mathbf{v}}_r) \otimes (\check{\gamma}_r \check{\mathbf{v}}_r) \quad (5a)$$

$$e_{sr}(\bar{\varphi}) = \text{vec}\{\mathbf{E}_{sr}(\bar{\varphi})\} = (\tilde{\gamma}_s \bar{\mathbf{G}}^T \bar{\mathbf{X}}(\bar{\varphi}) \tilde{\mathbf{v}}_s) \otimes (\check{\gamma}_r \check{\mathbf{v}}_r) \quad (5b)$$

$$e_{rs}(\ddot{\varphi}) = \text{vec}\{\mathbf{E}_{rs}(\ddot{\varphi})\} = (\tilde{\gamma}_r \tilde{\mathbf{v}}_r) \otimes (\check{\gamma}_s \ddot{\mathbf{G}} \ddot{\mathbf{X}}(\ddot{\varphi}) \check{\mathbf{v}}_s) \quad (5c)$$

$$e_{ss}(\bar{\varphi}, \ddot{\varphi}) = \text{vec}\{\mathbf{E}_{ss}(\bar{\varphi}, \ddot{\varphi})\} \\ = (\tilde{\gamma}_s \bar{\mathbf{G}}^T \bar{\mathbf{X}}(\bar{\varphi}) \tilde{\mathbf{v}}_s) \otimes (\check{\gamma}_s \ddot{\mathbf{G}} \ddot{\mathbf{X}}(\ddot{\varphi}) \check{\mathbf{v}}_s) \quad (5d)$$

we have

$$\mathbf{r} = \alpha \left(\underbrace{e_{rr} + e_{sr}(\bar{\varphi}) + e_{rs}(\ddot{\varphi}) + e_{ss}(\bar{\varphi}, \ddot{\varphi})}_{\mathbf{e}(\bar{\varphi}, \ddot{\varphi})} \right) + \mathbf{w} \quad (6)$$

where $\mathbf{w} = \text{vec}\{\mathbf{W}\}$ is a zero-mean circularity-symmetric Gaussian vector with covariance matrix⁴ $\sigma_w^2 \mathbf{I}_{\tilde{N}_r \tilde{N}_r}$. Notice that $\mathbf{e}(\bar{\varphi}, \ddot{\varphi})$ is the *spatial signature* of the prospective target; remarkably, it is verified by inspection that this vector possesses the following Kronecker structure

$$\mathbf{e}(\bar{\varphi}, \ddot{\varphi}) = \underbrace{(\tilde{\gamma}_r \tilde{\mathbf{v}}_r + \tilde{\gamma}_s \bar{\mathbf{G}}^T \bar{\mathbf{X}}(\bar{\varphi}) \tilde{\mathbf{v}}_s)}_{\bar{\mathbf{e}}(\bar{\varphi})} \otimes \underbrace{(\check{\gamma}_r \check{\mathbf{v}}_r + \check{\gamma}_s \ddot{\mathbf{G}} \ddot{\mathbf{X}}(\ddot{\varphi}) \check{\mathbf{v}}_s)}_{\bar{\mathbf{e}}(\ddot{\varphi})} \quad (7)$$

where $\bar{\mathbf{e}}(\bar{\varphi})$ is the *transmit signature*, resulting from the superposition of the direct and indirect transmit steering vectors with weights equal to the corresponding channels $\tilde{\gamma}_r$ and $\tilde{\gamma}_s$, and $\bar{\mathbf{e}}(\ddot{\varphi})$ is the *receive signature*, resulting from the

³We use here the term steering vector with some abuse of notation as the entries of $\bar{\mathbf{G}}^T \bar{\mathbf{X}}(\bar{\varphi}) \tilde{\mathbf{v}}_s$ and $\ddot{\mathbf{G}} \ddot{\mathbf{X}}(\ddot{\varphi}) \check{\mathbf{v}}_s$ may not have a unit-magnitude.

⁴The following developments can be also extended to the case where the covariance matrix of \mathbf{w} is full-rank and has the separable structure $\mathbf{E}[\mathbf{w}\mathbf{w}^H] = \bar{\mathbf{C}}_w \otimes \check{\mathbf{C}}_w$, with $\bar{\mathbf{C}}_w \in \mathbb{C}^{\tilde{N}_r \times \tilde{N}_r}$ and $\check{\mathbf{C}}_w \in \mathbb{C}^{\tilde{N}_s \times \tilde{N}_s}$.

superposition of the direct and indirect receive steering vectors with weights equal to the corresponding channels $\tilde{\gamma}_r$ and $\tilde{\gamma}_s$.

D. Channel model

While the design methodologies proposed next are general enough to remain independent of the adopted channel model, we will make at the analysis stage the following assumptions.

According to the standard radar equation [36], [37], we will model the channels $\tilde{\gamma}_r$, $\tilde{\gamma}_s$, $\tilde{\gamma}_r$, and $\tilde{\gamma}_s$ as follows

$$\tilde{\gamma}_r = \left(\frac{\bar{P}_r}{\bar{N}_r} \frac{\bar{G}(\bar{\theta}_t)}{4\pi\bar{\rho}^2\bar{L}_r} \right)^{1/2} e^{-i2\pi\bar{\rho}/\lambda} \quad (8a)$$

$$\tilde{\gamma}_s = \left(\frac{\bar{P}_r}{\bar{N}_r} \frac{\bar{G}(\bar{\theta}_s)\bar{\zeta}(\bar{\omega}_r, \bar{\omega}_t)}{(4\pi)^2\bar{\delta}^2\bar{d}^2\bar{L}_s} \right)^{1/2} e^{-i2\pi(\bar{\delta}+\bar{d})/\lambda} \quad (8b)$$

$$\tilde{\gamma}_r = \left(\frac{\check{G}(\check{\theta}_t)\lambda^2}{(4\pi)^2\check{\rho}^2\check{L}_r} \right)^{1/2} e^{-i2\pi\check{\rho}/\lambda} \quad (8c)$$

$$\tilde{\gamma}_s = \left(\frac{\check{I}_s \check{\zeta}(\check{\omega}_t, \check{\omega}_r)\check{G}(\check{\theta}_s)\lambda^2}{(4\pi)^3\check{d}^2\check{\delta}^2\check{L}_s} \right)^{1/2} e^{-i2\pi(\check{d}+\check{\delta})/\lambda} \quad (8d)$$

where $\bar{G}(\varphi)$ and $\check{G}(\varphi)$ are the gain of each transmit and receive element in the direction $\varphi = \{\varphi^{az}, \varphi^{el}\}$, respectively, $\bar{\zeta}(\varphi_{in}, \varphi_{out})$ and $\check{\zeta}(\varphi_{in}, \varphi_{out})$ are the bi-static RCS of each forward and backward reflecting element towards the direction $\varphi_{out} = \{\varphi_{out}^{az}, \varphi_{out}^{el}\}$ when illuminated from the direction $\varphi_{in} = \{\varphi_{in}^{az}, \varphi_{in}^{el}\}$, respectively, and \bar{L}_r , \bar{L}_s , \check{L}_r , and \check{L}_s are loss factors accounting for any additional attenuation along the corresponding paths, respectively.

Following [38]–[40], we will assume that

$$\bar{\zeta}(\varphi_{in}, \varphi_{out}) = \underbrace{\bar{A}_s \cos(\varphi_{in}^{az}) \cos(\varphi_{in}^{el})}_{\bar{\zeta}_a(\varphi_{in})} \times \underbrace{(4\pi\bar{A}_s/\lambda^2) \cos(\varphi_{out}^{az}) \cos(\varphi_{out}^{el})}_{\bar{\zeta}_g(\varphi_{out})}. \quad (9)$$

This is a simple yet realistic model, wherein the RCS of each element is regarded as the product of an effective receive aperture $\bar{\zeta}_a(\varphi_{in})$ and a transmit gain $\bar{\zeta}_g(\varphi_{out})$, with a cosine-shaped scan loss in both azimuth and elevation. This model treats the RIS as a reciprocal surface, i.e., $\bar{\zeta}(\varphi_{in}, \varphi_{out}) = \bar{\zeta}(\varphi_{out}, \varphi_{in})$; also, at broadside, the entire reflecting area is equal to the sum of the effective apertures of the building elements, so that the overall RIS behaves as a flat plate of area $N_s A_s$ [34]. The model in (9) will be also employed for $\check{\zeta}(\varphi_{in}, \varphi_{out})$ upon replacing \bar{A}_s with \check{A}_s .

Finally, following [35], the entries of \bar{G} will be modeled as⁵ $G_{nj} = 0$, if $\tilde{\gamma}_s = 0$, and

$$\bar{G}_{nj} = \left(\frac{\bar{G}(\bar{\theta}_{s,nj})\bar{\zeta}_a(\bar{\omega}_{r,nj})\bar{\delta}^2}{\bar{G}(\bar{\theta}_s)\bar{\zeta}_a(\bar{\omega}_r)\bar{\delta}_{nj}^2} \right)^{1/2} e^{-i2\pi(\bar{\delta}_{nj}-\bar{\delta})/\lambda} \quad (10)$$

otherwise. In this latter case, we have $\bar{G}_{nj} = 1$, if the j -th transmit and the n -th forward reflecting element are at the

⁵The path model in (8) and (10) can be farther generalized by considering a different bi-static RCS function for each element of the forward and backward RIS, which may be the case when the possible mutual coupling among the elements of the surface is accounted for.

center of their arrays, in keeping with (8). Similarly, \check{G} will be modeled as $\check{G}_{qn} = 0$, if $\tilde{\gamma}_s = 0$, and

$$\check{G}_{qn} = \left(\frac{\check{G}(\check{\theta}_{s,qn})\check{\zeta}_g(\check{\omega}_{r,qn})\check{\delta}^2}{\check{G}(\check{\theta}_s)\check{\zeta}_g(\check{\omega}_r)\check{\delta}_{qn}^2} \right)^{1/2} e^{-i2\pi(\check{\delta}_{qn}-\check{\delta})/\lambda} \quad (11)$$

otherwise.

III. SYSTEM DESIGN

Let $\mathbf{f} \in \mathbb{C}^{\bar{N}_r \times \bar{N}_r}$ be the unit-norm filter employed by the receiver to focus the radar towards the specific direction of the inspected resolution cell, which is under the designer's control; then, its output is

$$r = \alpha \mathbf{f}^H e(\bar{\varphi}, \bar{\varphi}) + \mathbf{f}^H \mathbf{w} \quad (12)$$

resulting in the following SNR

$$\text{SNR} = \frac{\sigma_\alpha^2}{\sigma_w^2} |\mathbf{f}^H e(\bar{\varphi}, \bar{\varphi})|^2 \quad (13)$$

where $\sigma_\alpha^2 = \text{E}[|\alpha|^2]$. Also, the GLRT discriminating between the target presence (hypothesis H_1) and absence (hypothesis H_0) is [41]

$$\frac{|r|^2}{\sigma_w^2} \underset{H_0}{\overset{H_1}{\geq}} \eta \quad (14)$$

where $\eta > 0$ is the detection threshold, to be set according to the desired probability of false alarm $P_{fa} = e^{-\eta}$; assuming that $|\alpha|^2$ is non fluctuating, exponentially distributed, or gamma distributed with variance $\sigma_\alpha^2/2$, the corresponding detection probabilities are [36], [37]

$$P_d = \begin{cases} Q_1(\sqrt{2\text{SNR}}, \sqrt{2\eta}) & \text{(non fluctuating)} \\ e^{-\eta/(1+\text{SNR})} & \text{(exponential)} \\ \left(1 + \frac{\gamma\text{SNR}/2}{(1+\text{SNR}/2)^2}\right) e^{-\eta/(1+\text{SNR}/2)} & \text{(gamma)}. \end{cases} \quad (15)$$

where $Q_1(\cdot, \cdot)$ is the Marcum's Q -function. The receive filter and the RIS phases can be jointly chosen to maximize the SNR at the cell under inspection and, as a by product, the detection probability in (15). For any $\bar{\varphi}$ and $\bar{\varphi}$, the optimal filter is the one matched to the signal to be detected, i.e.,

$$\mathbf{f} = \frac{e(\bar{\varphi}, \bar{\varphi})}{\|e(\bar{\varphi}, \bar{\varphi})\|}. \quad (16)$$

Hence, upon plugging (16) into (13), the optimal phases are obtained as the solution to

$$\max_{\bar{\varphi}, \bar{\varphi}} \|e(\bar{\varphi}, \bar{\varphi})\|^2. \quad (17)$$

We underline here that the above design is independent of the target and noise strength (namely, of σ_α^2 and σ_w^2); also, since the objective function $\|e(\bar{\varphi}, \bar{\varphi})\|^2 = \|\bar{e}(\bar{\varphi})\|^2 \|\check{e}(\bar{\varphi})\|^2$ and the constraint set in (17) are separable, the forward and backward phases can be optimized independently. Specifically, the problems to be solved are

$$\max_{\bar{\varphi}} \|\bar{e}(\bar{\varphi})\|^2 \quad (18)$$

when the forward RIS is present, and

$$\max_{\bar{\varphi}} \|\check{e}(\bar{\varphi})\|^2 \quad (19)$$

when the backward RIS is present.

A. Phase optimization

In this section we discuss the solution to (18); the following developments are easily adapted to also tackle the problem in (19) which indeed presents the same structure of (18). To proceed, let $\bar{\mathbf{y}} = \bar{\gamma}_r \bar{\mathbf{v}}_r$, $\bar{\mathbf{Q}} = \bar{\gamma}_s \bar{\mathbf{G}}^T \text{diag}(\bar{\mathbf{v}}_s)$, and $\bar{\mathbf{x}}(\bar{\varphi}) = (e^{i\bar{\varphi}_1} \dots e^{i\bar{\varphi}_{\bar{N}_s}})^T$; then, (18) can be rewritten as

$$\max_{\bar{\varphi}} \|\bar{\mathbf{y}} + \bar{\mathbf{Q}}\bar{\mathbf{x}}(\bar{\varphi})\|^2. \quad (20)$$

When $\text{Rank}(\bar{\mathbf{Q}}) = 1$, which occurs if the transmitter and the forward RIS are in each other's far-field (more on this in Sec. III-B) or $\bar{N}_r = 1$ or $\bar{N}_s = 1$, then the solution to (20) is derived in closed form. Indeed, upon factorizing $\bar{\mathbf{Q}}$ as $\bar{\mathbf{q}}_r \bar{\mathbf{q}}_s^T$, with $\bar{\mathbf{q}}_r \in \mathbb{C}^{\bar{N}_r}$ and $\bar{\mathbf{q}}_s \in \mathbb{C}^{\bar{N}_s}$, we have that

$$\begin{aligned} \|\bar{\mathbf{y}} + \bar{\mathbf{q}}_r \bar{\mathbf{q}}_s^T \bar{\mathbf{x}}(\bar{\varphi})\|^2 &= \left\| \bar{\mathbf{y}} + \bar{\mathbf{q}}_r \sum_{n=1}^{\bar{N}_s} |\bar{q}_{s,n}| e^{i(\bar{\varphi}_n + \angle \bar{q}_{s,n})} \right\|^2 \\ &= \|\bar{\mathbf{y}}\|^2 + \|\bar{\mathbf{q}}_r\|^2 \left| \sum_{n=1}^{\bar{N}_s} |\bar{q}_{s,n}| e^{i(\bar{\varphi}_n + \angle \bar{q}_{s,n})} \right|^2 \\ &\quad + 2\Re \left\{ \bar{\mathbf{y}}^H \bar{\mathbf{q}}_r \sum_{n=1}^{\bar{N}_s} |\bar{q}_{s,n}| e^{i(\bar{\varphi}_n + \angle \bar{q}_{s,n})} \right\} \\ &\leq \|\bar{\mathbf{y}}\|^2 + \|\bar{\mathbf{q}}_r\|^2 \left(\sum_{n=1}^{\bar{N}_s} |\bar{q}_{s,n}| \right)^2 + 2|\bar{\mathbf{y}}^H \bar{\mathbf{q}}_r| \sum_{n=1}^{\bar{N}_s} |\bar{q}_{s,n}| \end{aligned} \quad (21)$$

where the last upper bound is achieved when

$$\bar{\varphi}_n = -\angle \bar{q}_{s,n} - \angle(\bar{\mathbf{y}}^H \bar{\mathbf{q}}_r), \quad n = 1, \dots, \bar{N}_s. \quad (22)$$

When $\text{Rank}(\bar{\mathbf{Q}}) > 1$, instead, we proceed as follows. Upon introducing the positive semi-definite matrix⁶

$$\bar{\mathbf{B}} = \begin{pmatrix} \bar{\mathbf{Q}}^H \bar{\mathbf{Q}} & \bar{\mathbf{Q}}^H \bar{\mathbf{y}} \\ \bar{\mathbf{y}}^H \bar{\mathbf{Q}} & \|\bar{\mathbf{y}}\|^2 \end{pmatrix} \in \mathbb{C}^{(\bar{N}_s+1) \times (\bar{N}_s+1)} \quad (23)$$

the problem in (20) can be equivalently recast as

$$\max_{\bar{\varphi}, \bar{\phi}} \begin{pmatrix} e^{-i\bar{\phi}} \bar{\mathbf{x}}^H(\bar{\phi}) & e^{-i\bar{\phi}} \bar{\mathbf{B}} \\ e^{i\bar{\phi}} \bar{\mathbf{x}}(\bar{\phi}) & e^{i\bar{\phi}} \end{pmatrix}^T \quad (24)$$

which in turn is equivalent to

$$\begin{aligned} \max_{\bar{\mathbf{z}}} \quad & \bar{\mathbf{z}}^H \bar{\mathbf{B}} \bar{\mathbf{z}} \\ \text{s.t.} \quad & |\bar{z}_n| = 1, \quad n = 1, \dots, \bar{N}_s + 1. \end{aligned} \quad (25)$$

If $\bar{\mathbf{z}}^*$ solves (25), the solution to (20) can be recovered as $\bar{\varphi}_n = \angle \bar{z}_n^* - \angle \bar{z}_{\bar{N}_s+1}^*$, $n = 1, \dots, \bar{N}_s$. The problem (25) is a complex quadratic program, that has been shown to be strongly NP-hard in general [42]. A sub-optimal solution can be obtained via an alternate maximization, which iteratively optimizes one entry of $\bar{\mathbf{z}}$ at a time, as reported in Algorithm 1. Since $\bar{\mathbf{z}}^H \bar{\mathbf{B}} \bar{\mathbf{z}} = 2\Re\{\bar{z}_n^* \sum_{j \neq n} \bar{B}_{nj} \bar{z}_j\} + \bar{B}_{nn} |\bar{z}_n|^2 + \sum_{k \neq n} \sum_{j \neq n} \bar{z}_k^* \bar{B}_{kj} \bar{z}_j$, the maximization over \bar{z}_n gives

$$\bar{z}_n = \frac{\sum_{j \neq n} \bar{B}_{nj} \bar{z}_j}{\left| \sum_{j \neq n} \bar{B}_{nj} \bar{z}_j \right|} \quad (26)$$

if $\sum_{j \neq n} \bar{B}_{nj} \bar{z}_j \neq 0$, and any unit-modulus complex number, otherwise. Since the objective function is bounded above

⁶The positive-semidefiniteness is verified by exploiting the Schur complement for block matrices.

Algorithm 1 Alternate maximization for Problem (25)

- 1: Choose $\epsilon > 0$, $K_{\max} > 0$, and $\bar{\mathbf{z}} \in \mathbb{C}^{\bar{N}_s+1}$: $|\bar{z}_n| = 1$, $\forall n$
- 2: $k = 0$ and $\bar{f}_0 = \bar{\mathbf{z}}^H \bar{\mathbf{B}} \bar{\mathbf{z}}$
- 3: **repeat**
- 4: **for** $n = 1, \dots, \bar{N}_s + 1$ **do**
- 5: $\bar{z}_n = \begin{cases} \frac{\sum_{j \neq n} \bar{B}_{nj} \bar{z}_j}{\left| \sum_{j \neq n} \bar{B}_{nj} \bar{z}_j \right|}, & \text{if } \sum_{j \neq n} \bar{B}_{nj} \bar{z}_j \neq 0 \\ 1, & \text{otherwise} \end{cases}$
- 6: **end for**
- 7: $k = k + 1$
- 8: $\bar{f}_k = \bar{\mathbf{z}}^H \bar{\mathbf{B}} \bar{\mathbf{z}}$
- 9: **until** $(\bar{f}_k - \bar{f}_{k-1})/\bar{f}_k < \epsilon$ or $k = K_{\max}$

and monotonically increased at each iteration, convergence is ensured. The complexity per iteration is $\mathcal{O}(\bar{N}_s^2)$, with an initial cost of $\mathcal{O}(\bar{N}_s^3)$ to form the matrix $\bar{\mathbf{B}}$ in (23).

Alternatively, the problem in (25) can be reformulated as

$$\begin{aligned} \max_{\bar{\mathbf{Z}}, \bar{\mathbf{z}}} \quad & \text{Tr}(\bar{\mathbf{B}} \bar{\mathbf{Z}}) \\ \text{s.t.} \quad & \bar{Z}_{nn} = 1, \quad n = 1, \dots, \bar{N}_s + 1 \\ & \bar{\mathbf{Z}} \succeq 0, \quad \bar{\mathbf{Z}} = \bar{\mathbf{z}} \bar{\mathbf{z}}^H \end{aligned} \quad (27)$$

that admits the following (convex) relaxation

$$\begin{aligned} \max_{\bar{\mathbf{Z}}} \quad & \text{Tr}(\bar{\mathbf{B}} \bar{\mathbf{Z}}) \\ \text{s.t.} \quad & \bar{Z}_{nn} = 1, \quad n = 1, \dots, \bar{N}_s + 1, \quad \bar{\mathbf{Z}} \succeq 0. \end{aligned} \quad (28)$$

The above semi-definite program is well-studied in combinatorial optimization (see, e.g., the max-cut problem [43]) and can be solved by standard techniques, such as interior point methods, first-order methods on the associated dual problem, block coordinate ascent, etc. Once the matrix $\bar{\mathbf{Z}}^*$ solving (28) is found, a (sub-optimum) solution to (25) must be extracted. As in [42], [44], [45], we can generate a sample vector from a complex zero-mean circularly symmetric Gaussian distribution with covariance matrix $\bar{\mathbf{Z}}^*$ and normalize its entries to have a unit-magnitude, so as to obtain a sub-optimum solution $\bar{\mathbf{s}}$ for (25). This randomized algorithm satisfies a noticeable property [42], [46]. Indeed, let \bar{f}^* be the optimal value of the objective function in (25) and $\bar{f}_{\text{sub}}^* = \bar{\mathbf{s}}^H \bar{\mathbf{B}} \bar{\mathbf{s}}$; then, since $\bar{\mathbf{Z}}^*$ solves the relaxed problem in (28), we have that

$$\text{Tr}(\bar{\mathbf{B}} \bar{\mathbf{Z}}^*) \geq \bar{f}^* \geq \text{E}[\bar{f}_{\text{sub}}^*] = \text{Tr}(\bar{\mathbf{B}} \text{E}[\bar{\mathbf{s}} \bar{\mathbf{s}}^H]) = \text{Tr}(\bar{\mathbf{B}} F(\bar{\mathbf{Z}}^*)) \quad (29)$$

where $F(\bar{\mathbf{Z}}) \in \mathbb{C}^{(\bar{N}_s+1) \times (\bar{N}_s+1)}$ is the matrix with entry (i, j) defined as [42], [45]

$$\frac{1}{2} e^{i \angle \bar{Z}_{ij}} \int_0^\pi \cos(\varphi) \arcsin(|\bar{Z}_{ij}| \cos(\varphi)) d\varphi. \quad (30)$$

Therefore, since $\text{Tr}(\bar{\mathbf{B}} F(\bar{\mathbf{Z}}^*)) \geq \frac{\pi}{4} \text{Tr}(\bar{\mathbf{B}} \bar{\mathbf{Z}}^*)$ [42], we have

$$\text{Tr}(\bar{\mathbf{B}} \bar{\mathbf{Z}}^*) \geq \bar{f}^* \geq \text{E}[\bar{f}_{\text{sub}}^*] \geq \frac{\pi}{4} \text{Tr}(\bar{\mathbf{B}} \bar{\mathbf{Z}}^*) \quad (31)$$

which shows that this is a randomized $\frac{\pi}{4}$ -approximation algorithm.⁷ Clearly, multiple (independent) feasible points $\bar{\mathbf{s}}$ can be

⁷A (randomized) α -approximation algorithm is an algorithm that runs in polynomial time and produces a solution whose (expected) value is at least a fraction α of the optimum value [47].

computed, and the one providing the largest objective function in (25) can be chosen: in this case, the $\frac{\pi}{4}$ approximation ratio will not only hold in mean but also with a probability that goes to 1 exponentially fast with the number of samples.

B. Far-field deployment of the RIS

We study here in more detail the case where the transmit array and the forward RIS are in each other's far-field and the receive array and the backward RIS are in each other's far-field. In this situation, a plane wave approximation in the aforementioned radar-RIS hops can be made and, hence, the channel matrices in (10) and (11) simplify to $\bar{\mathbf{G}} = \bar{\mathbf{p}}_s \bar{\mathbf{p}}_r^T$ and $\check{\mathbf{G}} = \check{\mathbf{p}}_r \check{\mathbf{p}}_s^T$, respectively, where $\bar{\mathbf{p}}_r$ ($\check{\mathbf{p}}_r$) is the transmit (receive) steering vector of the radar towards the direction $\bar{\theta}_s$ ($\check{\theta}_s$) of the forward (backward) RIS, and $\bar{\mathbf{p}}_s$ ($\check{\mathbf{p}}_s$) is the transmit (receive) steering vectors of the forward (backward) RIS towards the direction $\bar{\omega}_r$ ($\check{\omega}_r$) of the radar transmitter (receiver); the vectors $\bar{\mathbf{p}}_r$, $\bar{\mathbf{p}}_s$, $\check{\mathbf{p}}_r$, and $\check{\mathbf{p}}_s$ are tied to the array geometry and have unit-magnitude entries. Since the matrix

$$\bar{\mathbf{Q}} = \underbrace{\bar{\mathbf{p}}_r}_{\bar{\mathbf{q}}_r} \underbrace{\bar{\mathbf{p}}_s^T \text{diag}(\bar{\mathbf{v}}_s) \bar{\gamma}_s}_{\bar{\mathbf{q}}_s^T} \quad (32)$$

has rank one, upon exploiting (21) and (22), we have that

$$\max_{\bar{\boldsymbol{\varphi}}} \|\bar{\mathbf{e}}(\bar{\boldsymbol{\varphi}})\|^2 = \bar{N}_r |\bar{\gamma}_r|^2 + \bar{N}_r \bar{N}_s^2 |\bar{\gamma}_s|^2 + 2\bar{N}_s |\bar{\gamma}_r^* \bar{\gamma}_s \bar{\mathbf{v}}_r^H \bar{\mathbf{p}}_r| \quad (33)$$

that is achieved when

$$\bar{\varphi}_n = -\angle(\bar{\gamma}_s \bar{p}_{s,n} \bar{v}_{s,n}) - \angle(\bar{\gamma}_r^* \bar{\mathbf{v}}_r^H \bar{\mathbf{p}}_r), \quad n = 1, \dots, \bar{N}_s. \quad (34)$$

Similarly, we have that

$$\max_{\check{\boldsymbol{\varphi}}} \|\check{\mathbf{e}}(\check{\boldsymbol{\varphi}})\|^2 = \check{N}_r |\check{\gamma}_r|^2 + \check{N}_r \check{N}_s^2 |\check{\gamma}_s|^2 + 2\check{N}_s |\check{\gamma}_r^* \check{\gamma}_s \check{\mathbf{v}}_r^H \check{\mathbf{p}}_r| \quad (35)$$

that is achieved when

$$\check{\varphi}_n = -\angle(\check{\gamma}_s \check{p}_{s,n} \check{v}_{s,n}) - \angle(\check{\gamma}_r^* \check{\mathbf{v}}_r^H \check{\mathbf{p}}_r), \quad n = 1, \dots, \check{N}_s. \quad (36)$$

To get some insights into the achievable performance, we now evaluate the optimal SNR under a LOS radar configuration (i.e., $\bar{\gamma}_r \check{\gamma}_r \neq 0$); from (7), (13), (33), and (35), we obtain

$$\begin{aligned} \text{SNR} &= \underbrace{\frac{\sigma_a^2 \bar{N}_r \check{N}_r |\bar{\gamma}_r \check{\gamma}_r|^2}{\sigma_w^2}}_{\text{SNR}_r} \\ &\times \underbrace{\left(1 + \bar{N}_s^2 \frac{|\bar{\gamma}_s|^2}{|\bar{\gamma}_r|^2} + 2\bar{N}_s \frac{|\bar{\gamma}_s|}{|\bar{\gamma}_r|} \frac{|\bar{\mathbf{v}}_r^H \bar{\mathbf{p}}_r|}{\bar{N}_r} \right)}_{\bar{\Gamma}_s} \\ &\times \underbrace{\left(1 + \check{N}_s^2 \frac{|\check{\gamma}_s|^2}{|\check{\gamma}_r|^2} + 2\check{N}_s \frac{|\check{\gamma}_s|}{|\check{\gamma}_r|} \frac{|\check{\mathbf{v}}_r^H \check{\mathbf{p}}_r|}{\check{N}_r} \right)}_{\check{\Gamma}_s} \end{aligned} \quad (37)$$

where SNR_r is the SNR when the radar operates alone, while $\bar{\Gamma}_s > 1$ and $\check{\Gamma}_s > 1$ are the gain granted by the RIS-aided illumination and observation, respectively. Under the model in (8), we have

$$\bar{\Gamma}_s \approx 1 + \bar{I}_s \frac{\bar{\mathcal{G}}(\bar{\theta}_s) \bar{L}_r \bar{N}_s^2 \bar{\zeta}(\bar{\omega}_r, \bar{\omega}_t)}{\bar{\mathcal{G}}(\bar{\theta}_t) \bar{L}_s 4\pi \bar{\delta}^2}$$

$$+ 2 \left(\bar{I}_s \frac{\bar{\mathcal{G}}(\bar{\theta}_s) \bar{L}_r \bar{N}_s^2 \bar{\zeta}(\bar{\omega}_r, \bar{\omega}_t)}{\bar{\mathcal{G}}(\bar{\theta}_t) \bar{L}_s 4\pi \bar{\delta}^2} \right)^{1/2} \frac{|\bar{\mathbf{v}}_r^H \bar{\mathbf{p}}_r|}{\bar{N}_r} \quad (38a)$$

$$\begin{aligned} \check{\Gamma}_s &\approx 1 + \check{I}_s \frac{\check{\mathcal{G}}(\check{\theta}_s) \check{L}_r \check{N}_s^2 \check{\zeta}(\check{\omega}_t, \check{\omega}_r)}{\check{\mathcal{G}}(\check{\theta}_t) \check{L}_s 4\pi \check{\delta}^2} \\ &+ 2 \left(\check{I}_s \frac{\check{\mathcal{G}}(\check{\theta}_s) \check{L}_r \check{N}_s^2 \check{\zeta}(\check{\omega}_t, \check{\omega}_r)}{\check{\mathcal{G}}(\check{\theta}_t) \check{L}_s 4\pi \check{\delta}^2} \right)^{1/2} \frac{|\check{\mathbf{v}}_r^H \check{\mathbf{p}}_r|}{\check{N}_r} \end{aligned} \quad (38b)$$

where the above approximations follow from the fact that $\bar{\rho} \approx \bar{d}$ and $\check{\rho} \approx \check{d}$, respectively. Observe now that, to ensure far-field operation, we must necessarily have $\bar{\delta} \lambda > 2\bar{D}_s^2$ and $\check{\delta} \lambda > 2\check{D}_s^2$ [33]; consequently, assuming that square RIS are employed, so that $\bar{N}_s \bar{A}_s = \bar{D}_s^2$ and $\check{N}_s \check{A}_s = \check{D}_s^2$, under the model in (9) we have

$$\frac{\bar{N}_s^2 \bar{\zeta}(\bar{\omega}_r, \bar{\omega}_t)}{4\pi \bar{\delta}^2} \leq \left(\frac{\bar{N}_s \bar{A}_s}{\bar{\delta} \lambda} \right)^2 \leq \frac{1}{4} \quad (39a)$$

$$\frac{\check{N}_s^2 \check{\zeta}(\check{\omega}_t, \check{\omega}_r)}{4\pi \check{\delta}^2} \leq \left(\frac{\check{N}_s \check{A}_s}{\check{\delta} \lambda} \right)^2 \leq \frac{1}{4}. \quad (39b)$$

From (38) and (39) we conclude that, when $\bar{\gamma}_r \check{\gamma}_r \neq 0$, the additional paths enabled by a far-field RIS deployment only provides a marginal SNR gain: the reason is that the reflecting area offered by the RIS cannot be sufficiently large to compensate for the signal attenuation experienced in the radar-RIS hop. As also confirmed by the analysis in Sec. IV, the forward (backward) RIS should rather be placed in the near-field of the radar transmit (receive) array, as close as possible, to significantly improve the system performance.

As a final remark, we point out that a far-field RIS deployment remains a competitive option whenever the indirect links allow to reach a spot that would otherwise remain blind [29].

C. Mono-static radar with a bi-directional RIS

We study here in more detail a mono-static radar wherein the same RIS helps both the transmitter and the receiver: in this case, we have $\bar{N}_s = \check{N}_s$, $(\bar{d}, \bar{\omega}_t) = (\check{d}, \check{\omega}_t)$, $\bar{\zeta}(\cdot, \cdot) = \check{\zeta}(\cdot, \cdot)$, $\bar{\mathbf{v}}_s = \check{\mathbf{v}}_s$, and $\bar{\gamma}_s \check{\gamma}_s \neq 0$. The disjoint design discussed in Section III-A can be directly employed if the phase shift introduced by each reflecting element can be reprogrammed in between the arrival of the forward (from the radar transmitter) and the backward (from the target) incident wave. To simplify the hardware, we also discuss next the relevant case where the additional constraint $\bar{\boldsymbol{\varphi}} = \check{\boldsymbol{\varphi}} = \boldsymbol{\varphi}$ is enforced to (17); accordingly, the phase design is recast as

$$\max_{\boldsymbol{\varphi}} \|e(\boldsymbol{\varphi}, \boldsymbol{\varphi})\|^2. \quad (40)$$

Notice that forcing $\bar{\boldsymbol{\varphi}} = \check{\boldsymbol{\varphi}}$ is optimal if $\bar{\mathbf{e}}(\cdot) = \check{\mathbf{e}}(\cdot)$: this occurs when the RIS is reciprocal *and* the radar employs the same reciprocal array for both transmission and reception; instead, it is inevitably sub-optimal if the system present an asymmetry between the transmit and the receive side. In this latter case, we propose to compute a sub-optimal solution to (40) by iteratively optimizing one phase shift at a time. To proceed, the objective function is expanded as

$$\|e(\boldsymbol{\varphi}, \boldsymbol{\varphi})\|^2 = \|\bar{\mathbf{t}}_n + \bar{\mathbf{q}}_n e^{i\varphi_n}\|^2 \|\check{\mathbf{t}}_n + \check{\mathbf{q}}_n e^{i\varphi_n}\|^2$$

Algorithm 2 Alternate maximization for Problem (40)

- 1: Choose $\epsilon > 0$, $K_{\max} > 0$, and $\{\varphi_n\}_{n=1}^{N_s}$
 - 2: $k = 0$ and $f_0 = 0$
 - 3: **repeat**
 - 4: $k = k + 1$
 - 5: **for** $n = 1, \dots, N_s$ **do**
 - 6: $\varphi_n = \arg \max_{\varphi} \Re\{A_n e^{i\varphi} + B_n e^{i2\varphi}\}$
 - 7: **end for**
 - 8: $f_k = \|e(\varphi, \varphi)\|^2$
 - 9: **until** $(f_k - f_{k-1})/f_k < \epsilon$ or $k = K_{\max}$
-

$$\begin{aligned}
 &= (\|\bar{\mathbf{t}}_n\|^2 + \|\bar{\mathbf{q}}_n\|^2) (\|\dot{\mathbf{t}}_n\|^2 + \|\dot{\mathbf{q}}_n\|^2) \\
 &\quad + 2(\|\bar{\mathbf{t}}_n\|^2 + \|\bar{\mathbf{q}}_n\|^2) \Re\{\dot{\mathbf{t}}_n^H \dot{\mathbf{q}}_n e^{i\varphi_n}\} \\
 &\quad + 2(\|\dot{\mathbf{t}}_n\|^2 + \|\dot{\mathbf{q}}_n\|^2) \Re\{\bar{\mathbf{t}}_n^H \bar{\mathbf{q}}_n e^{i\varphi_n}\} \\
 &\quad + 4\Re\{\dot{\mathbf{t}}_n^H \dot{\mathbf{q}}_n \bar{\mathbf{t}}_n^H \bar{\mathbf{q}}_n e^{i2\varphi_n}\} \quad (41)
 \end{aligned}$$

where $\bar{\mathbf{q}}_n$ is the n -th column of the matrix $\bar{\gamma}_s \bar{\mathbf{G}}^T \text{diag}(\bar{\mathbf{v}}_s)$, and $\bar{\mathbf{t}}_n = \bar{\gamma}_r \bar{\mathbf{v}}_r + \sum_{j=1, j \neq n}^{N_s} \bar{\mathbf{q}}_j e^{i\varphi_j}$ at the transmit side, and $\dot{\mathbf{q}}_n$ is the n -th column of the matrix $\dot{\gamma}_s \dot{\mathbf{G}} \text{diag}(\dot{\mathbf{v}}_s)$ and $\dot{\mathbf{t}}_n = \dot{\gamma}_r \dot{\mathbf{v}}_r + \sum_{j=1, j \neq n}^{N_s} \dot{\mathbf{q}}_j e^{i\varphi_j}$ at the receive side. Neglecting the irrelevant terms in (41), the problem to be solved becomes

$$\max_{\varphi_n} \Re\{A_n e^{i\varphi_n} + B_n e^{i2\varphi_n}\} \quad (42)$$

where $A_n = 2(\|\bar{\mathbf{t}}_n\|^2 + \|\bar{\mathbf{q}}_n\|^2) \dot{\mathbf{t}}_n^H \dot{\mathbf{q}}_n + 2(\|\dot{\mathbf{t}}_n\|^2 + \|\dot{\mathbf{q}}_n\|^2) \bar{\mathbf{t}}_n^H \bar{\mathbf{q}}_n$ and $B_n = 4\dot{\mathbf{t}}_n^H \dot{\mathbf{q}}_n \bar{\mathbf{t}}_n^H \bar{\mathbf{q}}_n$. The overall procedure is summarized in Algorithm 2: since the value of the objective function is bounded above and monotonically increased at each iteration, convergence is ensured. Finally, notice that the solution to (42) can be found among the zeros of the derivative of the objective function, i.e., $|A_n| \sin(\varphi_n + \angle A_n) + 2|B_n| \sin(2\varphi_n + \angle B_n)$, which can be obtained numerically.

D. More insights on the radar and RIS interplay

The radar can be focused on a different resolution cell in the illuminated region by only relying on receive signal processing; to be more specific, the range gating selects a region (namely, a circular or elliptical arc for a mono- and bi-static configuration, respectively) corresponding to a given propagation delay, while the subsequent spatial filter \mathbf{f} points towards a specific direction. When required, multiple resolutions cells can be simultaneously inspected by adjusting the gating time and the spatial filter. The achievable SNR in each resolution cell is tied to the set of emitted waveforms, the radiation pattern of the transmit/receive elements, and the array geometry. An RIS-aided radar system can now benefit from additional degrees of freedom, namely, the choice of the phase shifts of the reflecting elements. Since their response must be programmed before the transmission of the probing signal, the system engineer must decide in advance how the RISs should operate. Among the possible options, the design proposed in (17) aims at choosing the phase shifts so as to maximize the SNR at one specific resolution cell.⁸ The cell of interest can

⁸More generally, the forward and backward RISs could be pointed towards a different pair of resolution cells; also, they could be defocused to point towards multiple (widely-spaced or adjacent) resolution cells.

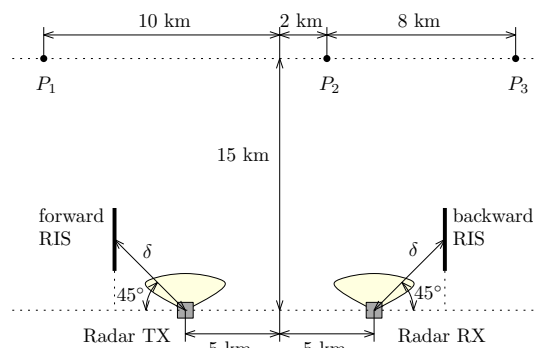


Figure 2. Considered system geometry.

be for example the one where an alert was previously found (if the radar is operating in an alert/confirm mode [48]) or the one where a previously-detected target is expected to be found (if the radar is operating in a tracking mode) or a particular spot that the system inspects on demand to prevent specific treats. Even if the RISs are optimized to look at a specific location, the radar can still continue to simultaneously inspect other resolution cells; we anticipate here that an SNR gain can as a by-product be obtained also in a large area close to the cell towards which the RISs have nominally been focused, as indicated by our examples in Sec. IV.

IV. NUMERICAL ANALYSIS

We present here some examples to demonstrate the performance achievable by an RIS-aided radar. The analysis is carried out under the model in Sec. II-D, with $\bar{L}_r = \bar{L}_s = \dot{L}_r = \dot{L}_s$ in (8). Also, Algorithms 1 and 2 are implemented with $K_{\max} = 200$, $\epsilon = 10^{-5}$, and a random initialization.

A. System geometry

We consider the geometry in Fig. 2, which features a bi-static radar operating at 5 GHz, aided by a forward and/or backward RIS. The local x and y axes of the transmit, receive, and reflecting arrays lays on the same plane, which also contains the prospective target. The transmitter and the receiver employ a linear array with a $\lambda/2$ element spacing along the local y -axis, $\bar{N}_r = 3$, and (unless otherwise stated) $\dot{N}_r = 8$; each array element has a rectangular shape of size $\lambda/2$ and λ along the local y and z axes, respectively, and a power pattern with a 3-dB beamwidth of 120° in azimuth and of 60° in elevation. The RISs (if present) have a square shape and are composed of $\bar{N}_s = \dot{N}_s = N_s$ adjacent square elements with area $\bar{A}_s = \dot{A}_s = \lambda^2/4$; also the center of these surfaces are located at the same distance $\bar{\delta} = \dot{\delta} = \delta$ from the array center of the transmitter and the receiver, respectively. According to (3), the minimum required separation between each transmit (receive) element and each forward (backward) reflecting element is 0.5 m. Finally, the target has an effective size of $\bar{D}_t = \dot{D}_t = 10\lambda$. Unless otherwise stated, we report next the performance when the target is at P_2 and the RISs are designed to maximize the SNR at this same location.

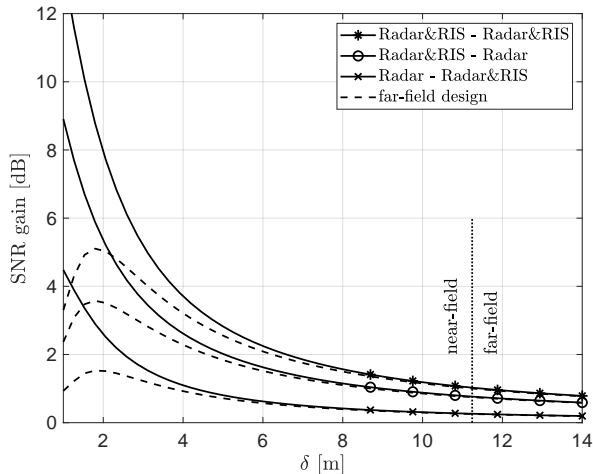


Figure 3. SNR gain (as compared to case where the radar operates alone) obtained by using a forward and/or a backward RIS versus δ , when $N_s = 225$. The system geometry in Fig. 2 is considered.

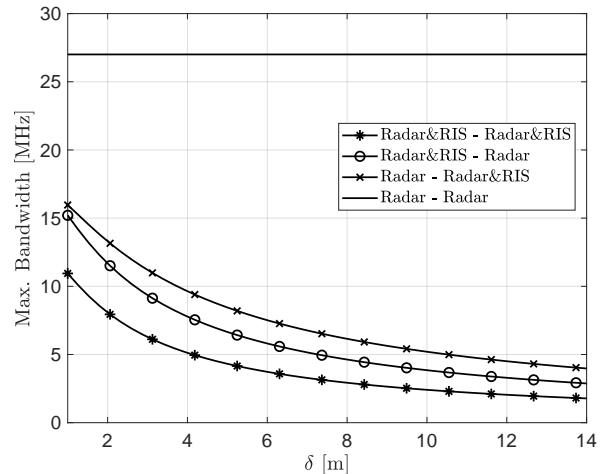


Figure 5. Maximum bandwidth ensuring that the delays of all target echoes reaching the receiver are not resolvable versus δ . The system geometry in Fig. 2 is considered.

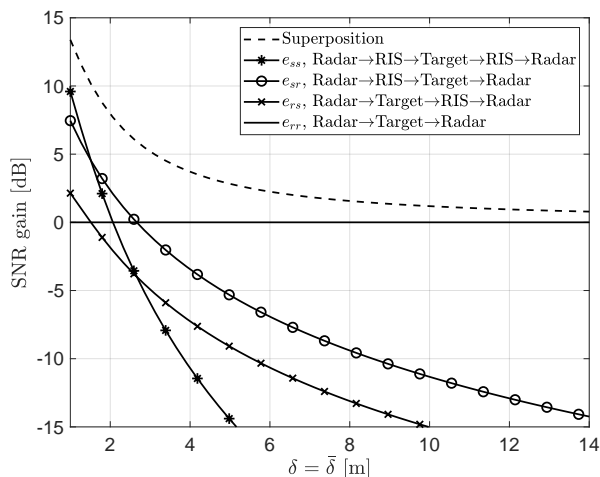


Figure 4. SNR gain (as compared to case where the radar operates alone) of the echoes e_{rr} , e_{rs} , e_{sr} , and e_{ss} and of their superposition versus δ , when both RIS are employed (“Radar&RIS - Radar&RIS” case) and $N_s = 225$. The system geometry in Fig. 2 is considered.

B. Impact of the radar-RIS distance

We first study the system behavior when δ is varied and $N_s = 225$. Fig. 3 reports the SNR gain obtained by using a forward and a backward RIS, a forward RIS only, and a backward RIS only, as compared to the case where the radar operates alone (i.e., only the direct echo e_{rr} exists): the configurations considered here correspond to the “Radar&RIS - Radar&RIS”, “Radar&RIS - Radar”, and “Radar - Radar&RIS” cases reported in Table I. As a benchmark, we include the performance obtained with the far-field design in (34) and (36). It is seen that a larger SNR gain is obtained when the radar and RIS get closer, and, in this regime, the far-field design turns out to be detrimental. The SNR gain becomes instead negligible when the radar and RIS arrays are located in each other’s far-field at both the transmit and the receive side, which in this example occurs when $\delta \geq 11.5$ m (as indicated by the vertical dotted line). Simultaneously using a forward and a backward

RIS almost doubles the gain as compared to using a single reflecting array. If only a single RIS has to be employed (e.g., due to cost constraints), then, for the considered scenario, it should be that at the transmit side: this is a consequence of the fact that the reflecting elements of the forward RIS offer a larger bi-static RCS towards P_2 than those of the forward counterpart. To get further insights, in Fig. 4 we consider the case where both RISs are simultaneously employed and report the SNR gain of the echoes e_{rr} , e_{rs} , e_{sr} , and e_{ss} and of their superposition. The echo e_{rs} is stronger than e_{sr} , in keeping with the fact that the elements of the forward RIS offer a larger bi-static RCS towards P_2 ; also, the echo e_{ss} is dominant when the distance between the radar and RIS arrays is very small, but it more rapidly fades out when δ is increased due to the more severe path-loss. Finally, Fig. 5 reports the maximum system bandwidth compatible with the required narrow-band assumption; this value have been computed as $(\tau_{\max} - \tau_{\min})/10$, where τ_{\max} and τ_{\min} are the maximum and the minimum propagation delays from the transmit to the receive elements. Not surprisingly, the maximum bandwidth decreases as δ and/or the number of hops are increased.

C. Impact of the RIS size

Next, we study the system behavior when the number of reflecting elements along each dimension, i.e., $\sqrt{N_s}$, is varied. Fig. 6 reports the SNR gain granted by the use of a forward and/or backward RIS, as compared to the case where the radar operates alone; not surprisingly, the gain increases as the reflecting surfaces get larger; however, it is important to notice that, as long as $\sqrt{N_s} < 8$, the radar and RIS arrays remain in each other’s far-field (as indicated by the vertical dotted line) and only marginal gains are obtained; when instead $\sqrt{N_s}$ gets larger, the advantage of using one or two RISs becomes evident. To further investigate this phenomenon, in Fig. 7 we consider the case where both RISs are simultaneously employed and report the SNR gain of the echoes e_{rr} , e_{rs} , e_{sr} , and e_{ss} and of their superposition. It is seen that the

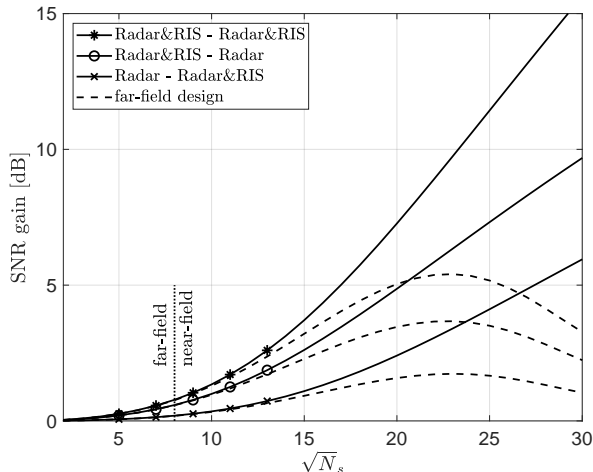


Figure 6. SNR gain (as compared to case where the radar operates alone) obtained by using a forward and/or a backward RIS versus $\sqrt{N_s}$, when $\delta = 4$ m. The system geometry in Fig. 2 is considered.

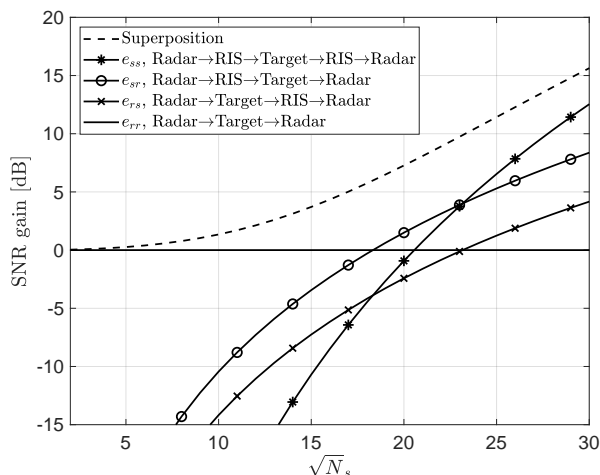


Figure 7. SNR gain (as compared to case where the radar operates alone) of each echoes e_{rr} , e_{rs} , e_{sr} , and e_{ss} and of their superposition versus $\sqrt{N_s}$, when $\delta = 4$ m, both RIS are employed (“Radar&RIS - Radar&RIS” case), and $N_s = 225$. The system geometry in Fig. 2 is considered.

indirect echoes become progressively stronger as the RIS size is increased and, eventually, dominate over the direct one; hence, upon fixing the distance from the radar, exploiting a reflecting surface becomes competitive only if its size is sufficiently large so as to positively balance the more severe attenuation over this path. In practice, the RIS size is limited by cost and installation constraints; also, it remains understood that complementing an existing radar with a one or more RISs can be attractive only if the cost is inferior to that of upgrading the radar itself with a better performing transceiver.

D. Impact of the target position

We now investigate the system performance as a function of the target position, which is moved along the line segment connecting P_1 to P_3 (from left to right), which has a length of 20 Km, when $N_s = 225$ and $\delta = 1$ m. At first, we assume that the RISs are designed to maximize the SNR at the

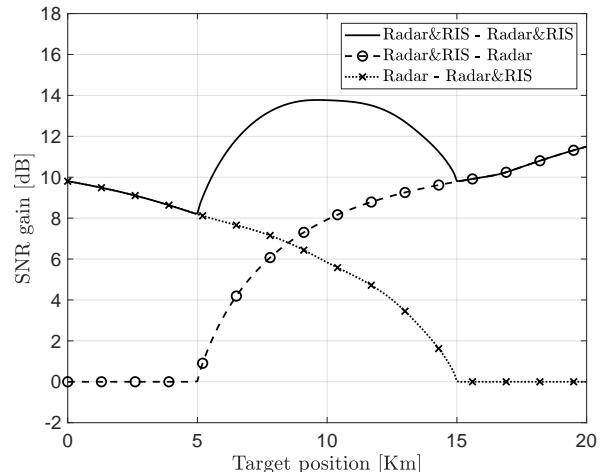


Figure 8. SNR gain (as compared to case where the radar operates alone) obtained by using a forward and/or a backward RIS versus the target position along the line segment going from P_1 ($= 0$ Km) to P_3 ($= 20$ Km), when $N_s = 225$ and $\delta = 1$ m. The system geometry in Fig. 2 is considered.

actual target location and, in Fig. 8, report the corresponding SNR gain. Notice that the forward RIS cannot illuminate the target in the interval $0 \div 5$ Km; accordingly, the “Radar&RIS–Radar” configuration does not provide any gain here, while the “Radar&RIS–Radar&RIS” and “Radar–Radar&RIS” configurations present the same gain. Similarly, the backward RIS cannot observe the target in the interval $15 \div 20$ Km; accordingly, the “Radar–Radar&RIS” is not effective here, while the “Radar&RIS–Radar&RIS” and “Radar&RIS–Radar” are equivalent. In between, the system can greatly benefit from the simultaneous use of two RISs, in keeping with the results shown in the previous examples: indeed, the RIS size is here sufficiently large with respect to the radar-RIS distance that the strength of the echo e_{ss} is significant. The observed asymmetry in the reported gains, with respect to the middle point of the line segment, is due to the fact that $\bar{N}_r \neq \check{N}_r$. Finally, Fig. 9 reports the performance when the RISs are designed to maximize the SNR at P_2 (marked here with a dotted vertical line); for comparison, it is also shown the achievable performance when the RISs are designed to maximize the SNR at the actual target location. Even under a mismatched design, a noticeable gain is observed across a large region around P_2 , which progressively reduces by moving away; the observed ripple is due to the fact that the direct and indirect echoes may not always add constructively at locations other than P_2 and, indeed, a small negative gain may even occur occasionally. Overall, the results in Fig. 9 reinforce the intuition that the system engineer can opportunistically activate the available reflecting surfaces to redirect part of the radiated/received power towards/from specific spots to locally boost the detection performance, while the radar transceiver can still keep looking at other regions with acceptable loss, which appears to be a nice feature.

E. Mono-static radar configuration

We assume here that the receive array is co-located with the transmit array and the same RIS is employed for both

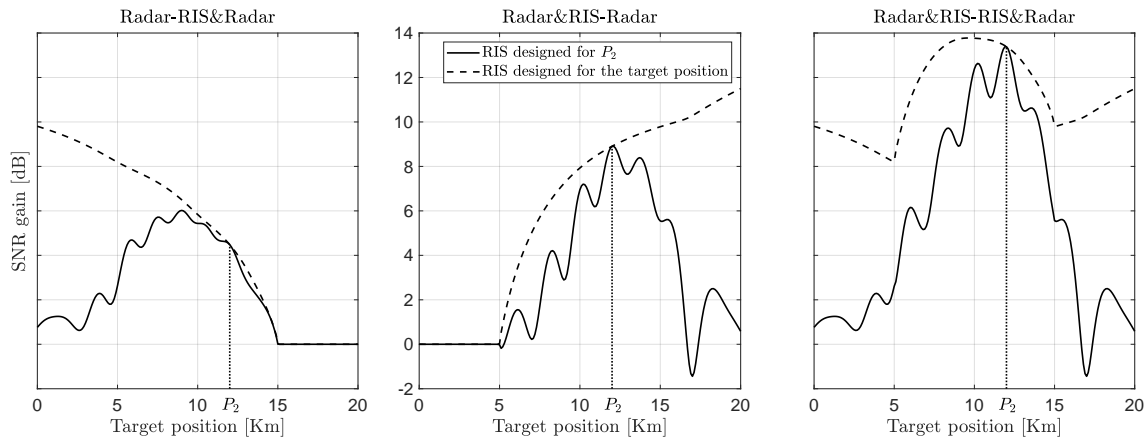


Figure 9. SNR gain (as compared to case where the radar operates alone) when using a forward RIS (left) or a backward RISs (center) or both RIS (right) versus the target position along the line segment going from P_1 ($= 0$ Km) to P_3 ($= 20$ Km), when $N_s = 225$ and $\delta = 1$ m. The RISs are designed to maximize the SNR at P_2 ($= 8$ Km) or at the actual target position. The system geometry in Fig. 2 is considered.

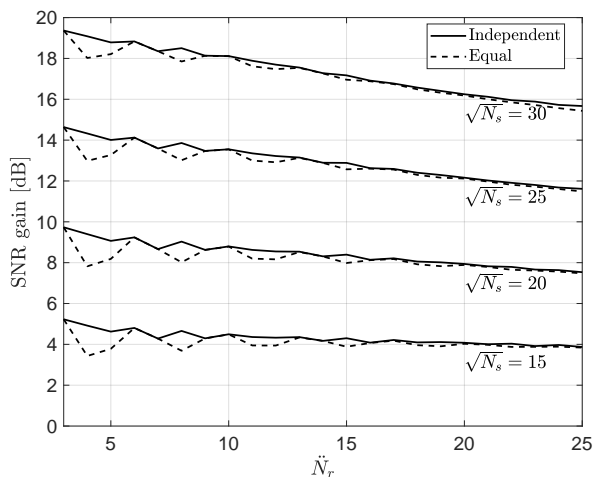


Figure 10. SNR gain (as compared to case where the radar operates alone) versus \tilde{N}_r , when the forward and backward phase shifts are independently optimized or are forced to be equal, $\sqrt{N_s} = 15, 20, 25, 30$ and $\delta = 4$ m. The system geometry in Fig. 2 is modified by moving the receiver to the same location of the transmitter and by using a single bi-directional RIS.

forward and backward reflection; all other parameters remain defined as in Sec. IV-A. Fig. 10 reports the SNR gain obtained when the forward and backward phases of each reflecting element are independently optimized or forced to be equal, as a function of the number of receive elements and for different RIS sizes, when $d = 4$ m. Remarkably, enforcing equal phase values only incurs marginal losses, thus simplifying the required hardware. Also, the obtained SNR gain reduces as \tilde{N}_r is increased; indeed, if the radar is equipped with a better receiver, the reward for using a nearby RIS will be less.

V. CONCLUSIONS

In this work we have started unveiling the benefits of complementing a MIMO radar with RISs placed close to the transmitter/receiver. We have derived a general signal model, which includes mono-static, bi-static, LOS, and NLOS radar configurations and accounts for the presence of up to four

paths from the transmitter to the prospective target to the receiver, and have recognized that the reflecting surfaces can be employed to enhance the achievable detection performance by redirecting/concentrating the radiated power towards/from specific spots. Our analysis have confirmed a simple intuition: an RIS should be better placed as close as possible to the radar transmitter/receiver in order to limit the additional path loss experienced by an indirect link, with a far-field deployment only providing a marginal advantage when the radar already has a direct view of the target. Also, in a mono-static configuration, the same surface can be used for both forward and backward reflection by simply maintaining the same phase shift, which greatly simplifies its construction and control.

Future works should study the effect of the clutter on the system design and might consider how to point the RISs towards multiple distinct spots (e.g. this might be useful for multi-target confirmation or tracking) or towards a wide region (e.g., this might be useful for target search). Also, the emitted waveforms and the RISs phase shifts could be jointly designed, so as to conveniently focus both the radar transceiver and the reflecting surfaces towards specific (not necessarily the same) regions. Future developments might also investigate applications involving a high-resolution radar where the direct and indirect echoes have resolvable delays or a passive/opportunistic radar exploiting an RIS to redirect the signal emitted by another (possibly non directional) source. A farther research line is studying if and how the estimation of the target parameters and the resolution of closely-spaced objects can improve in the presence of nearby RISs. Finally, the use of active RISs have recently been proposed for future 6G wireless communications [49], and their potential in the context of radar systems remains to be investigated.

REFERENCES

- [1] E. Basar *et al.*, "Wireless communications through reconfigurable intelligent surfaces," *IEEE Access*, vol. 7, pp. 116753–116773, 2019.
- [2] M. Di Renzo *et al.*, "Smart radio environments empowered by reconfigurable intelligent surfaces: How it works, state of research, and the road ahead," *IEEE Journal on Selected Areas in Communications*, vol. 38, no. 11, pp. 2450–2525, 2020.

- [3] Y. Liu *et al.*, “Reconfigurable intelligent surfaces: Principles and opportunities,” *IEEE Communications Surveys & Tutorials*, 2021.
- [4] S. Foo, “Liquid-crystal reconfigurable metasurface reflectors,” in *2017 IEEE International Symposium on Antennas and Propagation & USNC/URSI National Radio Science Meeting*, 2017, pp. 2069–2070.
- [5] C. Liaskos *et al.*, “Using any surface to realize a new paradigm for wireless communications,” *Communications of the ACM*, vol. 61, no. 11, pp. 30–33, 2018.
- [6] S. V. Hum and J. Perruisseau-Carrier, “Reconfigurable reflectarrays and array lenses for dynamic antenna beam control: A review,” *IEEE Transactions on Antennas and Propagation*, vol. 62, no. 1, pp. 183–198, 2013.
- [7] C. Huang *et al.*, “Reconfigurable intelligent surfaces for energy efficiency in wireless communication,” *IEEE Transactions on Wireless Communications*, vol. 18, no. 8, pp. 4157–4170, 2019.
- [8] C. Huang, G. C. Alexandropoulos, C. Yuen, and M. Debbah, “Indoor signal focusing with deep learning designed reconfigurable intelligent surfaces,” in *2019 IEEE 20th International Workshop on Signal Processing Advances in Wireless Communications (SPAWC)*, 2019, pp. 1–5.
- [9] H. Zhang, B. Di, L. Song, and Z. Han, “Reconfigurable intelligent surfaces assisted communications with limited phase shifts: How many phase shifts are enough?” *IEEE Transactions on Vehicular Technology*, vol. 69, no. 4, pp. 4498–4502, 2020.
- [10] R. Karasik, O. Simeone, M. Di Renzo, and S. Shamai Shitz, “Beyond max-SNR: Joint encoding for reconfigurable intelligent surfaces,” in *2020 IEEE International Symposium on Information Theory*, 2020, pp. 2965–2970.
- [11] J. Ye, S. Guo, and M.-S. Alouini, “Joint reflecting and precoding designs for ser minimization in reconfigurable intelligent surfaces assisted MIMO systems,” *IEEE Transactions on Wireless Communications*, vol. 19, no. 8, pp. 5561–5574, 2020.
- [12] G. C. Alexandropoulos and E. Vlachos, “A hardware architecture for reconfigurable intelligent surfaces with minimal active elements for explicit channel estimation,” in *2020 IEEE International Conference on Acoustics, Speech and Signal Processing*. IEEE, 2020, pp. 9175–9179.
- [13] Z. Zhou, N. Ge, Z. Wang, and L. Hanzo, “Joint transmit precoding and reconfigurable intelligent surface phase adjustment: A decomposition-aided channel estimation approach,” *IEEE Transactions on Communications*, 2020.
- [14] J. Mirza and B. Ali, “Channel estimation method and phase shift design for reconfigurable intelligent surface assisted MIMO networks,” *IEEE Transactions on Cognitive Communications and Networking*, 2021.
- [15] L. Zhao, Z. Wang, and X. Wang, “Wireless power transfer empowered by reconfigurable intelligent surfaces,” *IEEE Systems Journal*, 2020.
- [16] T. Hou *et al.*, “Reconfigurable intelligent surface aided NOMA networks,” *IEEE Journal on Selected Areas in Communications*, vol. 38, no. 11, pp. 2575–2588, 2020.
- [17] V. Jamali *et al.*, “Intelligent surface-aided transmitter architectures for millimeter-wave ultra massive mimo systems,” *IEEE Open Journal of the Communications Society*, vol. 2, pp. 144–167, 2021.
- [18] S. Zeng *et al.*, “Reconfigurable intelligent surface (RIS) assisted wireless coverage extension: RIS orientation and location optimization,” *IEEE Communications Letters*, vol. 25, no. 1, pp. 269–273, Jan. 2021.
- [19] H. Wymeersch *et al.*, “Radio localization and mapping with reconfigurable intelligent surfaces: Challenges, opportunities, and research directions,” *IEEE Vehicular Technology Magazine*, vol. 15, no. 4, pp. 52–61, Oct. 2020.
- [20] A. Elzanaty, A. Guerra, F. Guidi, and M.-S. Alouini, “Reconfigurable intelligent surfaces for localization: Position and orientation error bounds,” *arXiv:2009.02818*, 2020. [Online]. Available: <http://arxiv.org/abs/2009.02818>
- [21] A. Fascista, A. Coluccia, H. Wymeersch, and G. Seco-Granados, “RIS-aided joint localization and synchronization with a single-antenna mmwave receiver,” *arXiv:2010.14825*, 2020. [Online]. Available: <http://arxiv.org/abs/2010.14825>
- [22] K. Keykhosravi, M. F. Keskin, G. Seco-Granados, and H. Wymeersch, “SISO RIS-enabled joint 3D downlink localization and synchronization,” *arXiv:2011.02391*, 2020. [Online]. Available: <http://arxiv.org/abs/2011.02391>
- [23] J. He *et al.*, “Adaptive beamforming design for mmwave RIS-aided joint
- localization and communication,” in *2020 IEEE Wireless Communications and Networking Conference Workshops (WCNCW)*, 2020.
- [24] X. Wang *et al.*, “RIS-assisted spectrum sharing between MIMO radar and MU-MISO communication systems,” *IEEE Wireless Communications Letters*, 2020.
- [25] Z.-M. Jiang *et al.*, “Intelligent reflecting surface aided dual-function radar and communication system,” *IEEE Systems Journal*, 2021.
- [26] X. Wang, Z. Fei, Z. Zheng, and J. Guo, “Joint waveform design and passive beamforming for RIS-assisted dual-functional radar-communication system,” *IEEE Transactions on Vehicular Technology*, pp. 1–1, 2021.
- [27] S. Buzzi, E. Grossi, M. Lops, and L. Venturino, “Radar target detection aided by reconfigurable intelligent surfaces,” *Submitted to IEEE Signal Processing Letters*, 2021. [Online]. Available: <http://arxiv.org/abs/2104.00768>
- [28] A. Aubry, A. De Maio, and M. Rosamilia, “Reconfigurable intelligent surfaces for N-LOS radar surveillance,” *arXiv:2104.00456*, 2021. [Online]. Available: <http://arxiv.org/abs/2104.00456>
- [29] W. Lu *et al.*, “Intelligent reflecting surface-enhanced target detection in MIMO radar,” *IEEE Sensors Letters*, vol. 5, no. 2, pp. 1–4, 2021.
- [30] E. Björnson, O. Özdogan, and E. G. Larsson, “Reconfigurable intelligent surfaces: Three myths and two critical questions,” *IEEE Communications Magazine*, vol. 58, no. 12, pp. 90–96, 2020.
- [31] E. Fishler *et al.*, “Spatial diversity in radars – models and detection performance,” *IEEE Transactions on Signal Processing*, vol. 54, no. 3, pp. 823–838, Mar. 2006.
- [32] W. L. Stutzman and G. A. Thiele, *Antenna Theory and Design*, 3rd ed. New York, NY, USA: John Wiley Sons, 1998.
- [33] C. A. Balanis, *Advanced Engineering Electromagnetics*, 2nd ed. Hoboken, NJ, USA: Wiley, 2012.
- [34] B. Friedlander, “Localization of signals in the near-field of an antenna array,” *IEEE Transactions on Signal Processing*, vol. 67, no. 15, pp. 3885–3893, Aug. 2019.
- [35] C. P. Meyer and H. A. Mayer, *Radar target detection*. New York, NY, USA: Academic Press, 1973.
- [36] M. A. Richards, *Fundamentals of radar signal processing*, 2nd ed. New York, NY, USA: McGraw-Hill, 2005.
- [37] S. W. Ellingson, “Path loss in reconfigurable intelligent surface-enabled channels,” *arXiv:1912.06759*, 2019. [Online]. Available: <http://arxiv.org/abs/1912.06759>
- [38] W. Tang *et al.*, “Wireless communications with reconfigurable intelligent surface: Path loss modeling and experimental measurement,” *IEEE Transactions on Wireless Communications*, vol. 20, no. 1, pp. 421–439, Jan. 2021.
- [39] W. Tang *et al.*, “Path loss modeling and measurements for reconfigurable intelligent surfaces in the millimeter-wave frequency band,” *arXiv:2101.08607*, 2021. [Online]. Available: <http://arxiv.org/abs/2101.08607>
- [40] S. M. Kay, *Fundamental of Statistical Signal Processing: Detection Theory*. Prentice Hall, 1993, vol. II.
- [41] S. Zhang and Y. Huang, “Complex quadratic optimization and semidefinite programming,” *SIAM J. Optimization*, vol. 16, no. 3, pp. 871–890, 2006.
- [42] M. X. Goemans and D. P. Williamson, “Improved approximation algorithms for maximum cut and satisfiability problems using semidefinite programming,” *J. ACM*, vol. 42, no. 6, p. 1115–1145, Nov. 1995.
- [43] M. X. Goemans and D. P. Williamson, “Approximation algorithms for max-3-cut and other problems via complex semidefinite programming,” *J. Computer & System Sciences*, vol. 68, no. 2, pp. 442–470, 2004.
- [44] I. Waldspurger, A. d’Aspremont, and S. Mallat, “Approximation algorithms for max-3-cut and other problems via complex semidefinite programming,” *Math. Program.*, vol. 149, pp. 47–81, 2015.
- [45] A. M.-C. So, J. Zhang, and Y. Ye, “On approximating complex quadratic optimization problems via semidefinite programming relaxations,” *Math. Program.*, vol. 110, pp. 93–110, 2007.
- [46] D. S. Hochbaum, Ed., *Approximation Algorithms for NP-Hard Problems*. Boston, MA, USA: PWS Publishing Company, 1997.
- [47] E. Grossi, M. Lops, and L. Venturino, “Two-step sequential detection in agile-beam radars: Performance and tradeoffs,” *IEEE Transactions on Aerospace and Electronic Systems*, vol. 53, no. 5, pp. 2199–2213, Oct. 2017.
- [48] Z. Zhang *et al.*, “Active RIS vs. passive RIS: Which will prevail in 6G?” *arXiv:2103.15154*, 2021. [Online]. Available: <http://arxiv.org/abs/2103.15154>